Doped Mott insulator: Results from mean-field theory

Henrik Kajueter, Gabriel Kotliar, and Goetz Moeller
Department of Physics, Rutgers University, Piscataway, New Jersey 08855-0849
(Received 18 September 1995)

The Mott transition phenomena can be studied systematically in the limit of large lattice spatial coordination. We investigate the properties of doped Mott insulators with a variety of techniques and compare our results with experiments on transition-metal oxides. [S0163-1829(96)04524-9]

I. INTRODUCTION

The interaction-driven metal-insulator transition has fascinated theorists and experimentalists for many years. This transition is named after Sir Nevill Mott, who laid down the foundations of our physical understanding of this phenomenon.[1]

A periodic system having an odd number of electrons per unit cell must be an insulator (Mott insulator) when the electron-electron correlations are much larger than the bandwidth. In the limit of weak interactions band theory predicts the system to be metallic, so at some critical ratio of the interactions to the bandwith a metal-insulator transition, the Mott transition, must occur.

The detailed understanding of this phase transition, the Mott transition problem, has been elusive. It constitutes one of the most challenging problems in condensed-matter physics because of its nonperturbative nature. The absence of a natural small expansion parameter in the region near the transition makes this problem a test case study of nonperturbative many-body physics. The solution of this problem is a prerequisite for reaching a detailed understanding of the photoemission spectra and of the physical properties of transition-metal oxides.

The simplest model Hamiltonian exhibiting this phenomenon is the Hubbard model in the limit of large lattice coordination.[2] At half filling, this model captures many properties of real three-dimensional transition metal oxides and has allowed a thorough investigation of the pressure-driven Mott transition.[3–5] This work is relevant to the metal-insulator transition in NiS_xSe_{1-x},[6] $Ca_{1-x}Sr_xVO_3$,[7] and V_2O_3.[8–10]

The Mott transition can also be driven by changing the carrier concentration. This was realized experimentally in the ternary compounds $La_{1-x}Sr_xTiO_3$ (Ref. 11) and the $Y_{1-x}Ca_x TiO_3$ systems.[12,13] The simplest Hamiltonian describing this phenomenon is the Hubbard model away from half filling. In the limit of infinite dimensions, this Hamiltonian has been studied extensively by means of the quantum Monte Carlo method.[14–16] Good agreement between the predictions of the model and the experimental results of Tokura *et al.* was found.[15,14]

Very recently it has been established that doping a frustrated Mott insulator in the limit of large lattice coordination induces states inside the Mott-Hubbard gap.[17] This exact result, while restricted to infinitesimal doping, is a stringent test of the accuracy of the approximate techniques used to study correlated electrons in large dimensions. Here we reconsider the doped Hubbard model using, in addition to the projective self-consistent method, two complementary techniques, the exact diagonalization algorithm of Caffarel and Krauth,[18] and an extension of the iterative perturbation theory (IPT) introduced earlier by two of us.[26] By combining these two techniques we are able to explore larger values of the interaction parameters than those that have been treated so far and obtain a detailed picture of the correlated metallic regime in the proximity of the density-driven Mott transition.

At present there is no exact solution of the Hubbard model at zero temperature, even in the limit of infinite dimensions. To address this problem we use extensively two *approximate* methods mentioned above: the exact diagonalization and the recently proposed IPT scheme. The nature of the approximations in these two methods is of completely different origin: the exact diagonalization suffers from representing the bath of the Anderson model by a finite number of orbitals and the IPT is only an interpolation between exact limits ($U\rightarrow 0$, $t\rightarrow 0$, $\omega\rightarrow\infty$, and $\omega\rightarrow 0$). However, since both methods give almost identical results on the imaginary axis it is reasonable to trust the results thus obtained, at least as far as the trends on how various quantities evolve with doping are concerned.

The content of this paper is the following. Section II summarizes the methodology. In Sec. III we describe the phase diagram of the fully frustrated model. Then the evolution of the one-particle spectral density as a function of doping at zero temperature is discussed (Sec. IV). Section V addresses the doping dependence of the transfer of spectral weight by discussing the quasiparticle residue the compressibility, and the optical conductivity. Afterwards, we explore the magnetic susceptibility (Sec. VI) and subsequently some finite-temperature effects (Sec. VII). Section VIII discusses the Hall coefficient and the quasiparticle lifetime at very low temperatures. We conclude in Sec. IX with a discussion of the physical reasons why three-dimensional transition-metal oxides are well described by the mean-field formalism.

II. METHODOLOGY

The Hubbard Hamiltonian

$$H=-\sum_{\langle i,j\rangle}(t_{ij}+\mu)c^{\dagger}_{i,\sigma}c_{j,\sigma}+U\sum_i n_{i\uparrow}\cdot n_{i\downarrow} \qquad (1)$$

is the simplest, the ''bare bones'' model that captures the interplay of itinerancy and correlations. The hopping matrix elements t_{ij} in the limit of large spatial coordination, where a

typical site has m neighbors, are scaled as $t_{ij}\sim t/m^{\|i-j\|/2}$, so that the kinetic energy and the interactions remain finite for $m\to\infty$.[2]

As in our previous studies at half filling,[19,15] we consider lattices that have magnetic frustration, i.e., in the localized phase the spin degrees of freedom interact with magnetic exchange constants of different signs. The local bare density of states is assumed to be a semicircle

$$\rho_0(\epsilon)=\frac{2}{\pi D}\sqrt{1-\left(\frac{\epsilon}{D}\right)^2}, \tag{2}$$

with a half bandwidth $D=2t$. In this case one can realize the equations on a fully connected graph with random hopping matrix elements.[19,20]

The mean-field approach replaces the quantum many-body problem by a single-site quantum problem, an impurity model in an effective medium that is solved for self-consistently. Applying reliable techniques to the impurity model while implementing the self-consistency condition provides an accurate solution to the lattice problem.[3]

For the Hubbard model in the paramagnetic phase the associated impurity model is an Anderson model defined by the effective action

$$S_{\rm eff}[c,c^\dagger]=\sum_\sigma \int d\tau d\tau' c_\sigma^\dagger(\tau)G_0^{-1}(\tau-\tau')c_\sigma(\tau') + U\int_0^\beta d\tau n_{i\uparrow}(\tau)-n_{i\downarrow}(\tau). \tag{3}$$

The propagator G_0 plays the role of a Weiss field and, restricting to the paramagnetic phase, obeys the self-consistency condition

$$G_0^{-1}(i\omega_n)=i\omega_n+\Delta\mu-t^2G(i\omega_n)[G_0], \tag{4}$$

where $G(i\omega_n)=-\int_0^\beta e^{i\omega_n\tau}\langle T_\tau c(\tau)c^\dagger(0)\rangle_{S_{\rm eff}[G_0]}d\tau$ is a functional of $[G_0]$ and $\Delta_\mu:=\mu-\mu/2$. After self-consistency is attained, one can evaluate this functional at the self-consistent value of the Weiss field function to obtain the *local* Green's function of the Hubbard model.

The mean-field equations can be analyzed by a variety of methods. They range from qualitative arguments and analytic perturbative schemes to numerical methods based on quantum Monte Carlo,[5,21,15] exact diagonalization,[18,22,23] and iterative perturbation theory.[24,20,15] The projective self-consistent method[25] is applicable in an infinitesimal neighborhood of the transition and supplements the exact diagonalization studies. In this paper we will use the exact diagonalization algorithms to be able to make statements about rather large values of U. These are not accessible with conventional Monte Carlo algorithms because the expansion parameter in that technique is $U\Delta\tau$, where $\Delta\tau$ is the value of the imaginary time discretization parameter τ. The exact diagonalization technique yields, on the real axis, only a discrete set of poles for the spectral function as a result of treating only a finite number of particles in the corresponding impurity model. Therefore we supplement these results with an iterative perturbation scheme, which on the imaginary axis is in good agreement with the exact diagonalization results[26] and in addition yields smooth spectra on the real axis. For completeness, this method will be presented briefly in the next subsection.

A. IPT away from half filling

We now describe the perturbation scheme we use to supplement the exact diagonalization results. The approach[26] is in the spirit of the iterative perturbation theory introduced in Refs. 24 and 3 and similar to other schemes.[27,30] The key idea is to search for a self-energy as a functional of the ''Weiss field'' such that the self-energy expression becomes exact both in the weak- and in the strong-coupling limit. Moreover, it should have the correct behavior at both small and large frequencies. The naive extension of the method originally proposed for half filling fails to give reasonable results for finite doping. However, we propose a generalization to arbitrary filling by constructing a self-energy expression that has the correct behavior in the limits discussed above. Our ansatz for the self-energy is given by

$$\Sigma^{(2)}(\omega)=Un+\frac{\frac{n(1-n)}{n_0(1-n_0)}\tilde\Sigma_0^{(2)}(\omega)}{1-\frac{(1-n)U-\mu+\tilde\mu_0}{n_0(1-n_0)U^2}\tilde\Sigma_0^{(2)}(\omega)}. \tag{5}$$

Here $\tilde\Sigma_0^{(2)}(\omega)$ is the normal second-order contribution to the self-energy

$$\tilde\Sigma_0^{(2)}(\omega)=U^2\int_{-\infty}^0 d\epsilon_1\int_0^\infty d\epsilon_2 d\epsilon_3\frac{\rho^{(0)}(\epsilon_1)\rho^{(0)}(\epsilon_2)\rho^{(0)}(\epsilon_3)}{\omega+\epsilon_1-\epsilon_2-\epsilon_3-i\eta} + U^2\int_0^\infty d\epsilon_1\int_{-\infty}^0 d\epsilon_2 d\epsilon_3\frac{\rho^{(0)}(\epsilon_1)\rho^{(0)}(\epsilon_2)\rho^{(0)}(\epsilon_3)}{\omega+\epsilon_1-\epsilon_2-\epsilon_3-i\eta}, \tag{6}$$

where $\rho^{(0)}=(1/\pi)\,{\rm Im}\tilde G_0$. The (advanced) Green's function $\tilde G_0(\omega)$ is defined by

$$\tilde G_0(\omega):=\frac{1}{\omega+\tilde\mu_0-t^2G(\omega)}. \tag{7}$$

While n marks the physical particle number (obtained from G), n_0 is a fictitious particle number determined from G_0. The parameter $\tilde\mu_0$ is chosen such that the Luttinger theorem is fulfilled:

$$\mu_0=\mu-\Sigma^{(2)}[\tilde\mu_0](\omega=0)\,,\quad \mu_0:=\mu|_{U=0}. \tag{8}$$

The self-consistency is closed by

$$G^{-1}(\omega)=\tilde G_0^{-1}(\omega)-\tilde\mu_0+\mu-\Sigma^{(2)}(\omega)\,. \tag{9}$$

For the numerical implementation it is more convenient to fix $\tilde\mu_0$ (rather than μ). Then, starting with a guess for G and μ, one can compute $\tilde G_0$, n, and n_0. Afterward, (5) yields $\Sigma^{(2)}(\omega)$ and we obtain a new μ from the Luttinger theorem. The loop is closed by (9) and the iteration continued until convergence is achieved.

In the case of half filling the procedure reduces to ordinary IPT. Therefore, we are dealing with an extension of this method to finite doping.

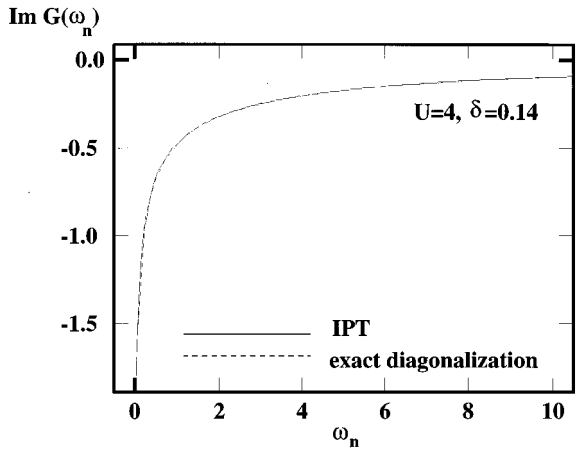

FIG. 1. Im$G(\omega)$ at $T=0$ for $U=4D$ and hole doping $\delta=0.14$: iterative perturbation theory (full line) vs exact diagonalization (dashed line).

Expression (5) becomes exact in the atomic limit and is correct to order U^2 in the weak-coupling limit. The proper large-frequency behavior is related to the fact that the spectral moments up to quadratic order are reproduced exactly.[28,29] The correct zero-frequency behavior is ensured by satisfying the Luttinger theorem. This is the main difference from an earlier scheme[30] using related ideas and is essential to obtain good agreement with the exact diagonalization results.

To test the validity of our method we compare it with results obtained using the exact diagonalization algorithm of Caffarel and Krauth.[18] Both methods are in close agreement when used on the imaginary axis (see Fig. 1). The advantage of the present IPT scheme is seen on real axis: In Fig. 2 we display the spectral functions obtained by these two methods. Although the exact diagonalization is doing its best in producing the correct spectral distribution it is unable to give a smooth density of states. Instead several δ peaks occur as a consequence of treating only a finite number of orbitals in the Anderson model. The iterative perturbation scheme in contrast yields a continuous plot. In this sense it supplements the exact diagonalization.

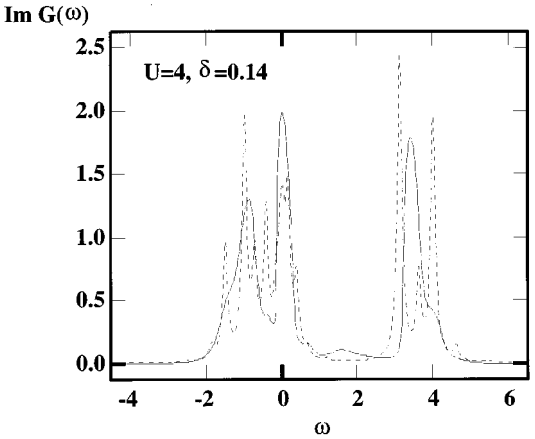

FIG. 2. Im$G(\omega)$ at $T=0$ for $U=4D$ and hole doping $\delta=0.14$: iterative perturbation theory (full line) vs exact diagonalization (dashed line).

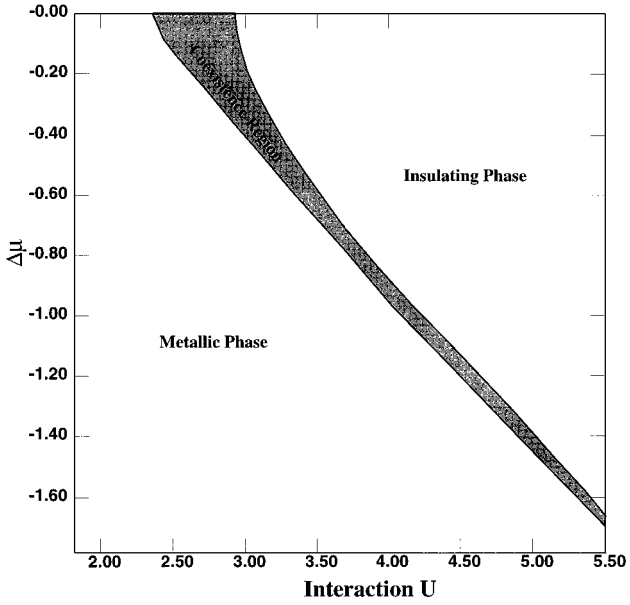

FIG. 3. Phase diagram in the μ-U plane of the Hubbard model on a fully frustrated lattice at zero temperature (exact diagonalization).

III. PHASE DIAGRAM

The phase diagram of the half-filled model displays a coexistence region in the temperature interaction strength plane. For *given* noninteger *average occupancy* and in the paramagnetic phase of the fully frustrated model, there is only one solution of the mean-field equations. As function of chemical potential, however, there is a region of coexistence of two solutions that describe a doped metal and an insulator. The phase diagram in the μ-U plane of the Hubbard model on a fully frustrated lattice at zero temperature is shown in Fig. 3. It was obtained by exact diagonalization with eight sites for $U=4$ by looking for the region where an insulating solution with zero density of states at zero energy coexists with the metallic solution having a finite low-energy density of states. For the particle-hole symmetric case a detailed description of this procedure can be found in Ref. 22. The shaded area denotes the region of parameter space where the mean-field equations have two different solutions: one metallic and the other insulating.

Following the technique discussed in Ref. 22, we measured the energy of each solution and determined that through the coexistence region the metallic solution is the lowest in energy. This is in agreement with the analytic argument presented in Refs. 25 and 17. The region of coexistence is also in good agreement with the completely independent determination of the phase diagram by means of the projective self-consistent method.[17]

IV. EVOLUTION OF THE SPECTRAL DENSITY AS A FUNCTION OF DOPING

In this section we discuss the evolution of the spectral function as one dopes the Mott insulator. It has been shown[17] that for infinitesimal doping, new states are created in the Mott-Hubbard gap. The states in the doped system have no

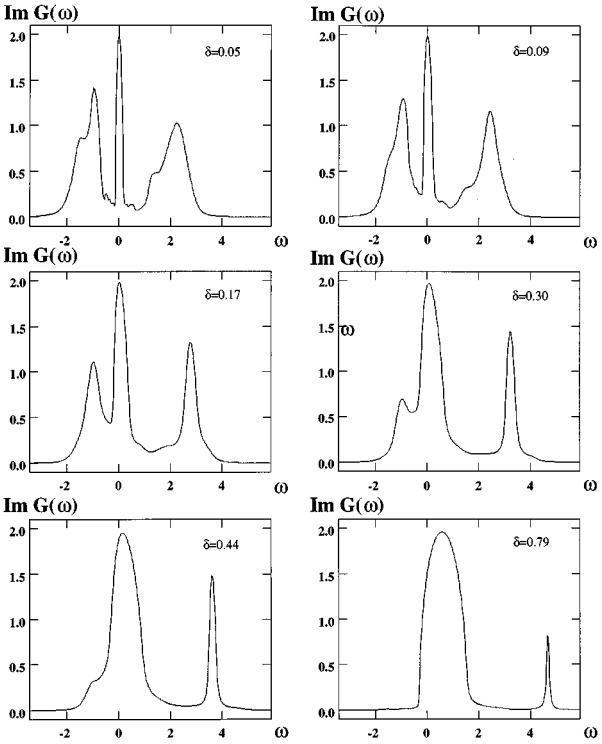

FIG. 4. Evolution of the spectral function as one dopes the Mott insulator for $U=3$ (IPT).

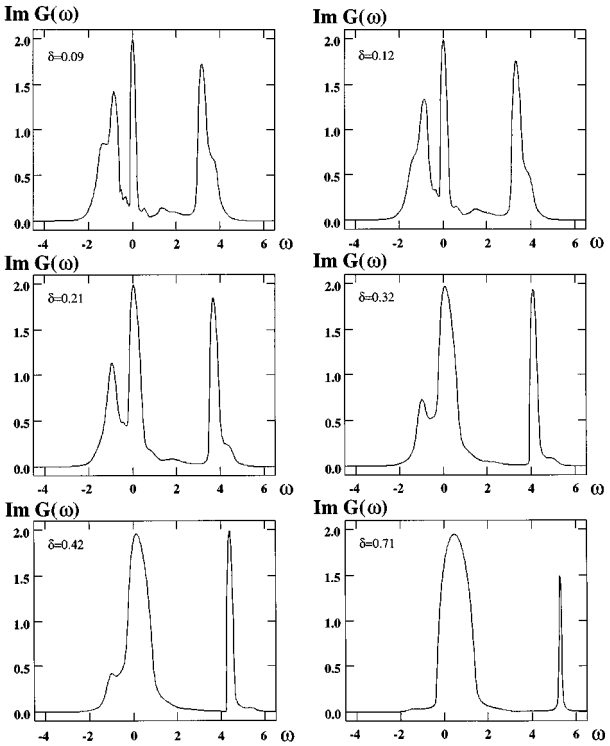

FIG. 5. Evolution of the spectral function as one dopes the Mott insulator for $U=4$ (IPT).

simple relation to those that existed in the insulator. This physical picture is similar to that obtained by the slave boson treatment.[31,32] Notice that the results of the large- d approach are in closer agreement with Ref. 32 than with Ref. 31.

Since the projective self-consistent method is restricted to infinitesimal doping it is important to ask at which doping the resonance merges with the Hubbard band and, more generally, how the spectral function evolves as one dopes a Mott insulator. We address these and other questions below.

In Figs. 4 and 5 we show the evolution of the spectral function of the Hubbard model as obtained from IPT for $U=3$ and 4. Figure 6 displays exact diagonalization results for $U=10$. For small doping the resonance peak is well separated from the lower Hubbard band. But once the doping is increased, the resonance moves quickly inside the band and the qualitative results are very similar to those obtained with the slave boson method.[31,32]

The position of the resonance as a function of doping can be related to the different physical regimes of the corresponding Anderson impurity model.[3] For small doping the lattice sites are predominantly single occupied. There are virtually no charge fluctuations and the system is in the *local moment regime* dominated by quantum fluctuations between the $|\uparrow\rangle$ and the $|\downarrow\rangle$ states. In this case the resonance is well separated from the lower Hubbard band.

With increasing doping charge fluctuations between single occupied and empty states become important (*mixed valence regime*). The resonance merges into the lower Hubbard band.

Once the particle density gets so small that the lattice sites are predominantly empty, the *empty orbital regime* is reached. At this point the characteristic resonance peak loses its identity and the spectral function resembles that of the noninteracting system.

The crossover from the local moment to the mixed valence regime is quite fast, as can be seen in Fig. 7. Here the three regimes were distinguished by computing the expectation values $n_{\text{single}}=\Sigma_\sigma\langle(1-n_\sigma)n_{\bar{\sigma}}\rangle$ and $n_{\text{empty}}=\langle(1-n_\sigma)(1-n_{\bar{\sigma}})\rangle$. As a criterion for the single moment regime we chose $n_{\text{single}}>0.9$, while the empty orbital regime was determined from $n_{\text{empty}}>0.8$.

V. DOPING DEPENDENCE OF THE TRANSFER OF SPECTRAL WEIGHT

As one dopes the Mott insulator with holes, spectral weight is transferred from the upper Hubbard band to the resonance near the Fermi level. As the weight of the resonance grows the quasiparticle residue Z increases and consequently the mass enhancement is reduced. The divergence of the effective mass as the doping is decreased was established in earlier publications.[22,16] In this section we discuss various aspects of the doping dependence of the quasiparticle residue and of the integrated spectral weight, such as their dependence on U/D for values of U that were not accessible to the quantum Monte Carlo method.

The evolution of the weight in the upper Hubbard band w_+ as a function of doping is shown in Fig. 8 for different values of U. The transfer of spectral weight can be parametrized as $w_+\approx 1/2-a(U)\delta$ for $U>U_c$. This relation holds for dopings up to a maximum value $\tilde{\delta}$, which increases as a function of U ($\tilde{\delta}\approx 0.04$ for $U=3.5$ and $\tilde{\delta}\approx 0.1$ for $U=5$). When U is infinite, $a(U)$ is equal to 0.5 and increases as

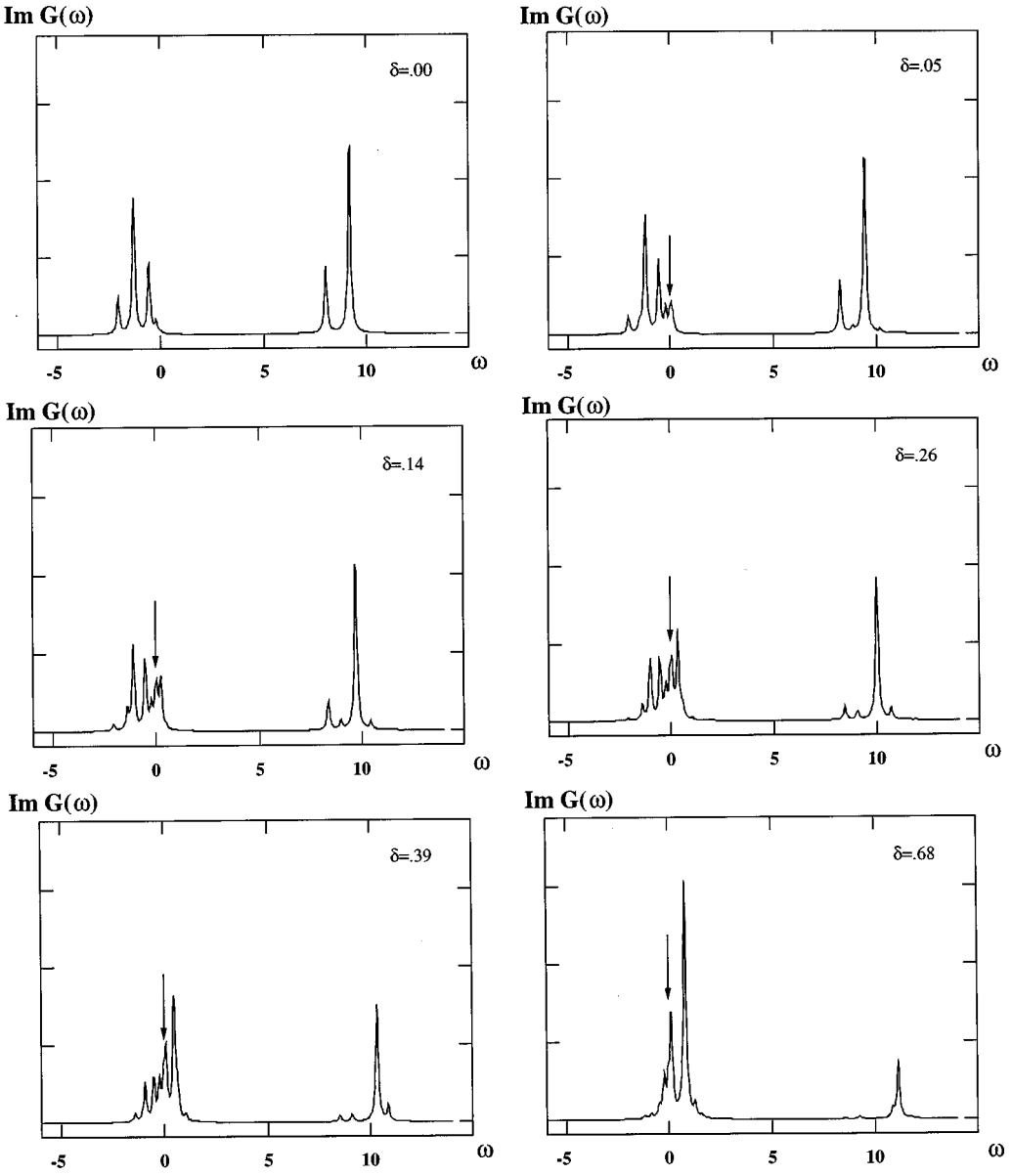

FIG. 6. Evolution of the spectral function as one dopes the Mott insulator for $U=10$ (exact diagonalization with eight sites). The arrows indicate the position of the resonance peak.

U is reduced. These results are qualitatively similar to what is observed in exact diagonalization studies of the *finite-dimensional* Hubbard model.[33]

The control parameter of the transition is the deviation of the chemical potential from its critical value μ_c. That is, the weight w in the resonance behaves as $w \sim(\mu-\mu_c)(\mu_c-U/2)$ for $U>U_c$. To convert from chemical potential to doping one needs the particle number as a function of μ. This relation is displayed in Fig. 9.

The compressibility for infinitesimal doping is in general finite, but vanishes at U_c. The density as a function of chemical potential near half filling can be parametrized as

$$\delta=A_0+A_1\left(\mu-\frac{U}{2}\right)+A_2\left(\mu-\frac{U}{2}\right)^2. \qquad (10)$$

δ denotes a small doping. The coefficients A_i depend on U: A_0 vanishes below U_c and increases (decreases) quickly for hole (electron) doping, when U is increased above U_c. Moreover, $A_1\approx\alpha_1(U-U_c)$. The parameter A_2 is always positive and increases as a function of U. This increase is faster above, rather than below, U_c.

Above U_c, the critical region where the parametrization (10) is applicable is relatively small (typically $\delta\leqslant 0.01$). However, it increases as U is lowered below U_c ($\delta\leqslant 0.05$ for $U=2$).

The compressibility is nonsingular (except when U approaches U_c). This implies that $w\sim\delta$, i.e., the weight w of the resonance at zero frequency increases as a function of doping.

To analyze the low-energy, low-temperature thermodynamics, one has to investigate the properties of the states that

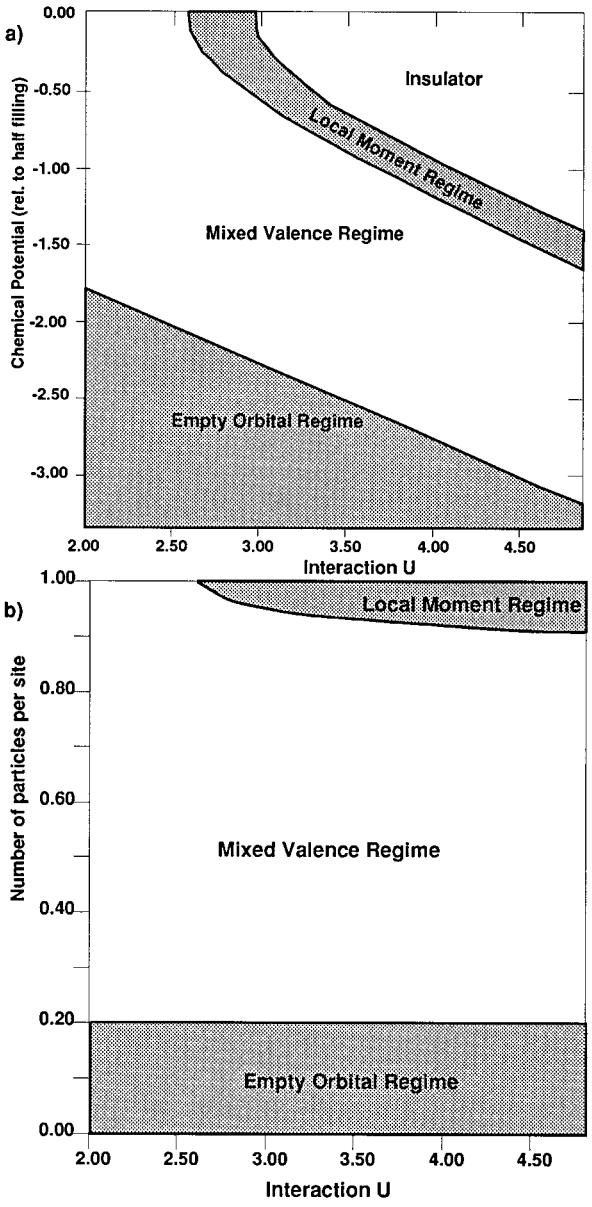

FIG. 7. Different regimes of the Hubbard model (see the text): (a) U-$\delta\mu$ plane and (b) U-n plane.

form the low-energy resonance. The Mott transition as a function of doping is driven by the low-energy spectral weight w, which drives the quasiparticle residue Z to zero as the doping vanishes as long as the interaction is above its critical value. Z is in general proportional to w, but smaller than this quantity. In infinite dimensions the vanishing of Z implies the divergence of the effective mass and consequently the vanishing of the renormalized Fermi energy $\epsilon_F = DZ$.

The quasiparticle residue increases as a function of doping. It is sketched in Fig. 10 for different values of U. With the projective self-consistent method one can demonstrate that $Z = b(U)w$, where $b(U)$ is a weak function of U that equals approximately 0.5 at $U=3$ and 0.3 at $U=8$.

A different measure of transfer of spectral weight appears in the optical spectra. The optical conductivity of the model at $T=0$ can be represented as

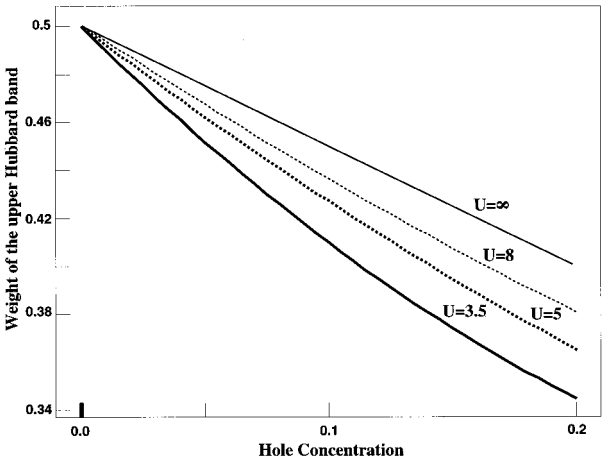

FIG. 8. Weight of the upper Hubbard band w_+ as a function of doping for various values of the interaction U (data from exact diagonalization).

$$\sigma(\omega) = \frac{\omega_P^{*2}}{4\pi}\delta(\omega) + \sigma_{\mathrm{reg}}(\omega), \tag{11}$$

where the coefficient in front of the δ function is the Drude weight and ω_P^* is the renormalized plasma frequency. The Drude weight and the integrated optical spectral weight evolve as a function of doping. In infinite dimensions the Drude weight is simply related to Z (Refs. 10 and 14) via $\omega_P^{*2}/4\pi = (4\pi t^2 e^2 a^2/\hbar^2 \nu)\, Z\rho^0(0)$ The integrated optical weight is proportional to the kinetic energy $\langle T \rangle$. Figure 11 shows this quantity as a function of doping for different values of U. Notice that at half filling the kinetic energy is finite and of the order of the magnetic exchange. For small values of U the results are in excellent agreement with the results of Monte Carlo calculations obtained earlier.[14]

VI. SUSCEPTIBILITY

The inverse magnetic susceptibility χ_S^{-1} has been investigated in various publications and is easily understood not to

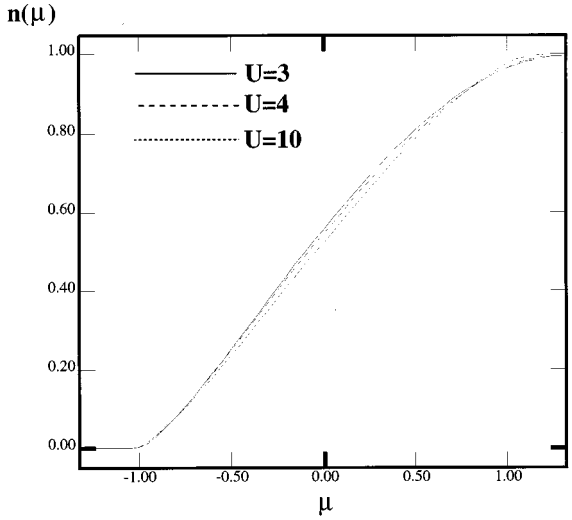

FIG. 9. Particle number versus the chemical potential for different values of the interaction U (exact diagonalization).

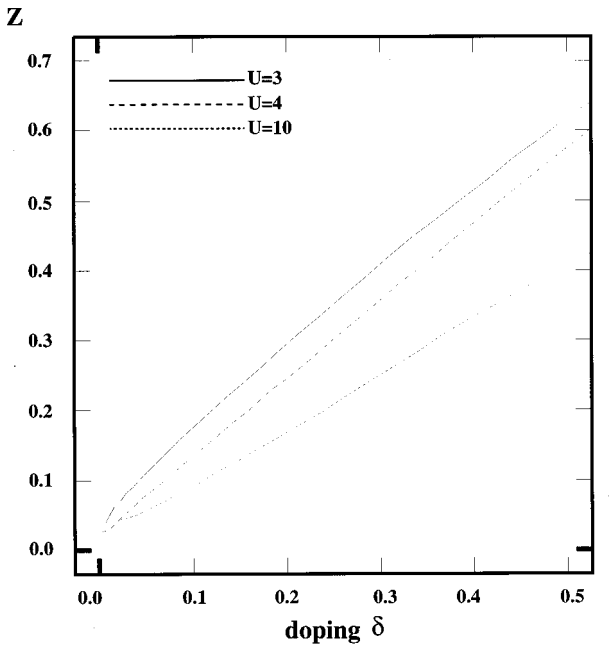

FIG. 10. Quasiparticle residue Z as a function of doping for various values of the interaction (exact diagonalization, with an effective temperature $T_{\text{eff}}=0.01$).

be divergent near half filling using the arguments of Ref. 22. The exact diagonalization results near the transition are found to be consistent with the parametrization

$$\chi_S^{-1} \approx c(U)w + J, \tag{12}$$

with $c(U)$ depending weakly on U. In the insulating phase $\chi_S^{-1} \approx (J+T)$. Equation (12) indicates that the magnetic susceptibility remains finite at the transition due to the existence of a nonzero superexchange constant $J = 2t^2/U = D^2/2U$.

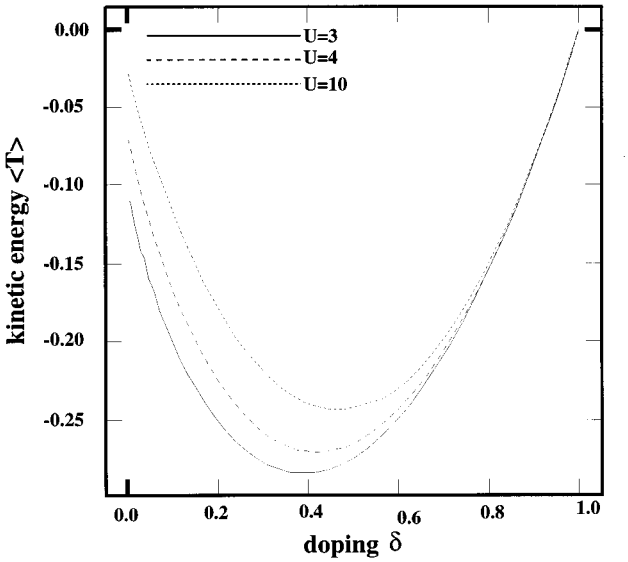

FIG. 11. Kinetic energy as a function of doping (exact diagonalization).

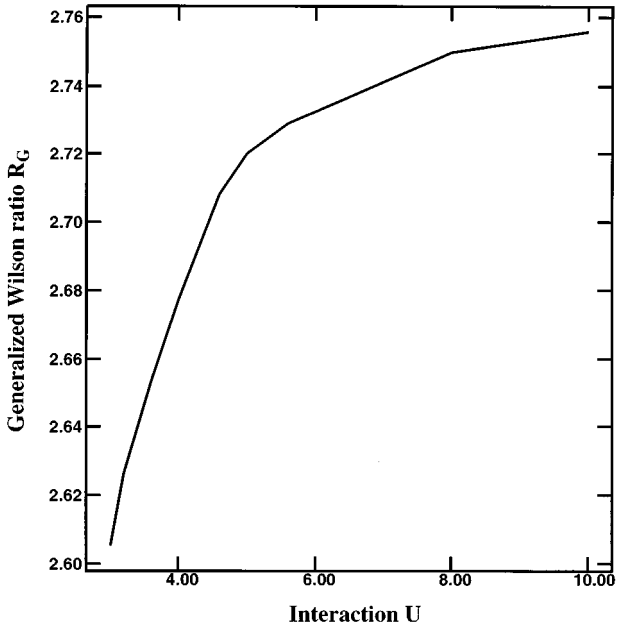

FIG. 12. Generalized Wilson ratio R_g for infinitesimal doping as a function of the interaction U (results from exact diagonalization).

This should be contrasted with the behavior of the local spin susceptibility (in units of $g\mu_B/2$), which diverges as the Mott transition is approached:

$$\chi_{\text{loc}}^{-1} \approx d(U)w. \tag{13}$$

The coefficient $d(U)$ decreases slowly with U and is given by 0.12 at $U=3$ and falls to 0.07 at $U=8$. This leads us to the definition of a generalized Wilson ratio R_g defined as the ratio of χ_{loc}/γ to its noninteracting ($U=0$) value $\chi_{\text{loc0}}/\gamma_0$ [where $\chi_{\text{loc0}} = 16/3\pi D\,(g\mu_B/2)^2$ and $\gamma_0 = 4\pi k_B^2/(3D)$]. R_g measures the enhancement of the susceptibility at a generic q in the Brillouin zone. It increases very slightly as U increases: $R_g=2.6$ for $U=3$ and $R_g=2.75$ for $U=10$. A plot of this quantity vs U obtained with the projective self-consistent method is shown in Fig. 12.

VII. CROSSOVER AT FINITE TEMPERATURES

The infinite U Anderson impurity model is known to have a Kondo resonance. Here we study the Hubbard model in the intermediate-U regime where a resonance peak is also present. This analogy[3] is particularly useful for understanding the temperature dependence of the local spectral function. From the theory of the Anderson impurity model it is known that there exists a scale T_0, the Kondo energy, above which the electrons and the impurity are weakly coupled and below which a resonance at the Fermi level is formed. Two important issues are the dependence of the coherence temperature T_0 on physical parameters of the Hubbard model and the nature of the crossover between the high-temperature and the low-temperature regime in this model.

Jarrell and collaborators have addressed some of these issues in Refs. 16 and 34. They investigated the evolution of the spectral function and other physical properties as function of temperature using the Monte Carlo method and the maximum-entropy technique. Here we address this problem

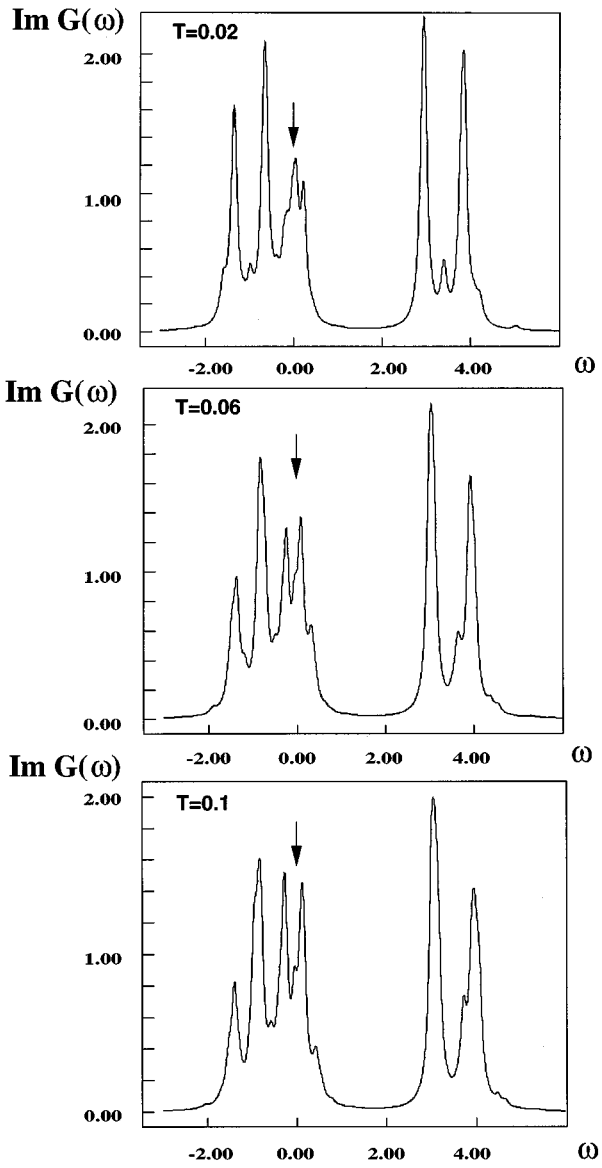

FIG. 13. Evolution of the spectral function as a function of temperature displaying the temperature dependence of the resonance peak. A six-site exact diagonalization was used for $\delta=0.075$ and $U=4$.

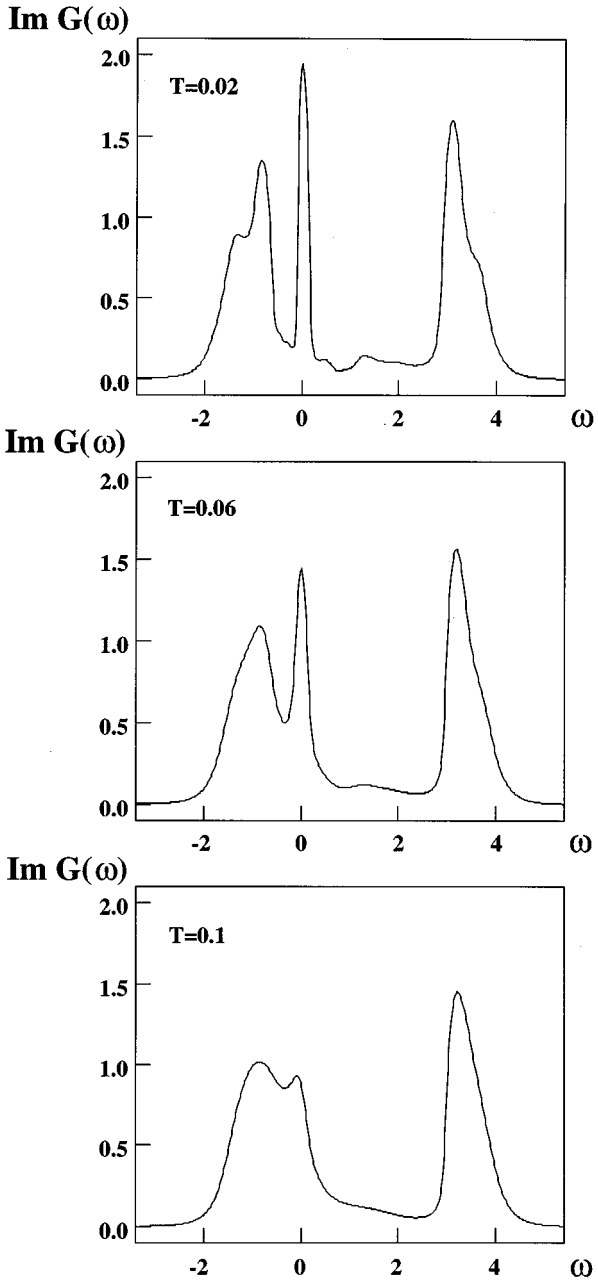

FIG. 14. Spectral function for different temperatures as obtained from IPT for $U=4$ and $\delta=0.075$.

using exact diagonalization and some analytic considerations.

Figure 13 displays the temperature dependence of the spectral function as obtained from an exact diagonalization calculation for $U=4$ and $\delta=0.075$. For comparison, we plotted the corresponding IPT results in Fig. 14. Both figures display the decay of the resonance peak with increasing T.

The temperature dependence of the local spin susceptibility χ_{loc} is shown in Fig. 15. It has the form $\chi_{\mathrm{loc}}=1/\alpha T+T_0$, where α increases with increasing doping ($\alpha\approx 1.1$ for $\delta=0.06$ and $\alpha\approx 1.3$ for $\delta=0.4$) so that there is no universal scaling function describing the temperature dependence of χ as in the single impurity model. The increase of α as doping increases has a simple physical interpretation since the doping decreases the effective magnetic moment per site.

The parameter T_0 defines again the coherence temperature below which Fermi liquid theory is applicable. For small doping we find $T_0=\alpha\delta^{3/2}$. This relation holds up to $\delta\approx 0.14$ for $U=4$ (with $\alpha\approx 0.5D$), as shown in Fig. 16.

One can understand this unusual dependence of the coherence temperature on doping by a simple energetic argument. We construct a free-energy functional of the coherence parameter w, the weight in the resonance. At zero temperature it gives the energy difference between the metallic and the insulating phase and is proportional to δ^2. A concrete realization of the energy functional is $E(w)=(\mu-\mu_c)w+bw^2$. Its minimization results in an energy difference that is proportional to $(\mu-\mu_c)^2$, i.e., to the square of the doping. At finite temperatures, one has to include entropy effects. For

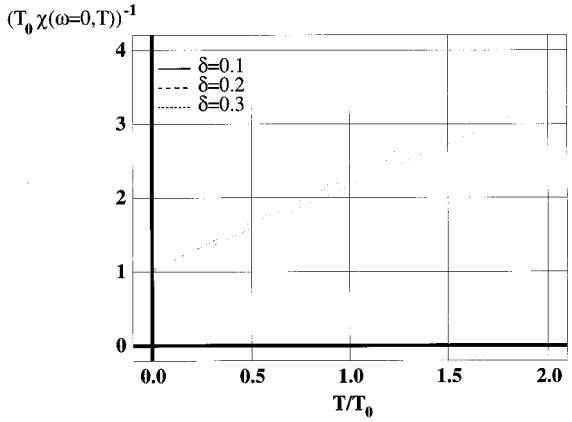

FIG. 15. Temperature dependence of the inverse local spin susceptibility. Plot of $[T_0\chi_{\rm loc}(\omega=0,T)]^{-1}$ as a function of T/T_0. Results from exact diagonalization with $U=4$ and 6 sites.

a Fermi system with a Fermi energy ϵ_F, the entropy per lattice site is approximately constant ($\approx S_0$) when $T \gg \epsilon_F$, while at low temperatures $S \approx T/\epsilon_F$. So we can parametrize the entropy by $S \approx S_0 \tanh(T/wDS_0)$. Balancing this entropy against the energy difference, which is of order δ^2, sets the crossover scale $T_0 \sim \delta^{3/2}$.

Interestingly, T_0 is considerably smaller than the renormalized Fermi energy $\epsilon_F = ZD$ (e.g., $T_0/ZD \approx 0.12$ for $\delta = 0.1$).

The existence of a low-energy scale and the associated anomalous temperature dependence of the spectral function cause a strong variation of the number of particles as a function of temperature for fixed chemical potential. This is displayed in Fig. 17.

The observed temperature dependence is due to two competing effects. (a) In the metallic correlated regime, spectral weight is transferred from the resonance to the lower Hubbard band as the temperature increases. Since the chemical potential is kept fixed, this causes an increase in the particle number. (b) As the temperature increases some holes are

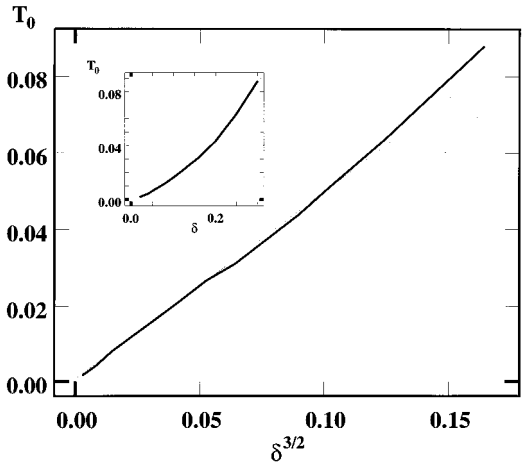

FIG. 16. Doping dependence of the coherence temperature for $U=4$: T_0 as a function of $\delta^{3/2}$ (thick line). The thin line was obtained by fitting $T=\alpha\delta^{3/2}$ to the exact diagonalization data for $\delta \leqslant 0.14$. The inset shows $T_0(\delta)$.

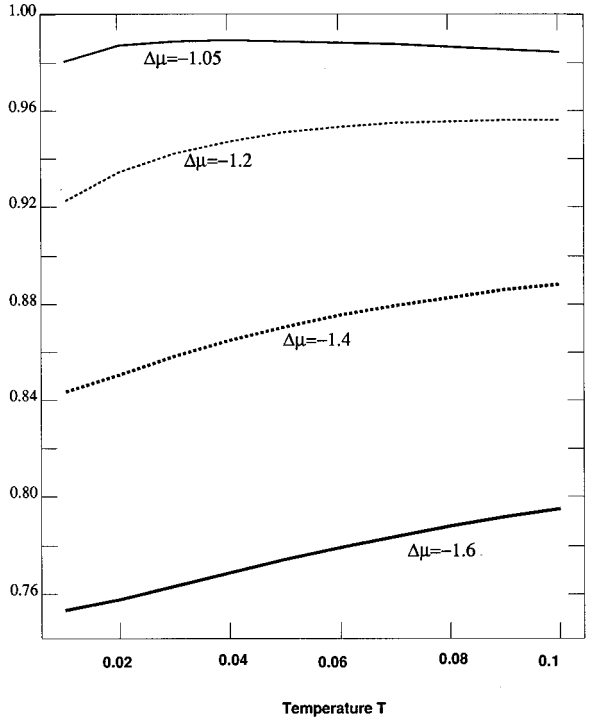

FIG. 17. Particle number per site as a function of temperature for $U=4$ and $\Delta\mu=\mu-(U/2)=-1.05,-1.2,-1.4,-1.6$ using exact diagonalization with $5+1$ orbitals.

thermally activated and the number of particles decreases. This effect is the only effect present in the insulating phase ($\mu > \mu_c$) and dominates in the metallic state very near the metal insulator transition at higher temperatures.

It has been emphasized in Refs. 16 and also in 35 that in a wide temperature range the resistivity of the doped Hubbard model is linear and it is suggested that the crossover from the Fermi liquid regime is very slow. Here we investigate this issue further and conclude that the crossover behavior from the Fermi liquid regime is actually quite rapid. Figure 18 displays the behavior of the resistivity and the scattering rate as a function of temperature for $U=3$ and $\delta=0.25$.

Both quantities change their behavior at the scale T_0. Moreover, the resistivity has a wide linear region that is due to a saturation in the scattering rate. Notice that this regime occurs well above T_0 where the crossover has already taken place.

VIII. LOW-TEMPERATURE LIFETIMES AND THE HALL COEFFICIENT

It is also interesting to study the behavior of the lifetime as obtained from the imaginary part of the retarded self-energy. It is quadratic in frequency and has a stronger divergence than the quasiparticle residue. Defining $\Delta = wD$, we obtain using the projective self-consistent method following Refs. 25 and 17

$$\mathrm{Im}\Sigma(\omega + i0^+, T) = -\frac{s(U)D}{\Delta^2}(\omega^2 + \pi T^2). \qquad (14)$$

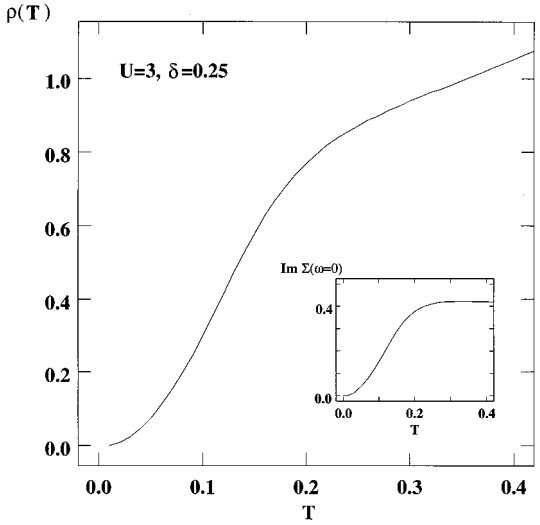

FIG. 18. Resistivity and self-energy as a function of temperature for $U=3$ and $\delta=0.25$ (IPT).

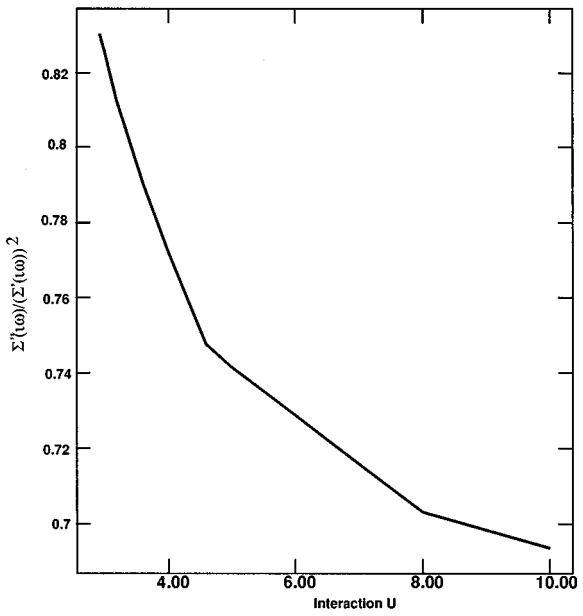

FIG. 19. $[\partial^2\Sigma/(\partial\omega)^2]/(\partial\Sigma/\partial\omega)^2|_{\omega=0}$ for infinitesimal doping as a function of the interaction (exact diagonalization). The ratio is proportional to A/γ^2.

$s(U)$ increases slowly as U increases varying from 1.4 at $U=3$ to 3.3 at $U=8$.

A related quantity is the low-temperature resistivity. In mean-field theory, we write

$$\rho(T)=\left(\frac{\omega_{p0}}{2\pi}\right)^{-2} 2\ \mathrm{Im}\Sigma(T)=AT^2, \tag{15}$$

where the plasma frequency of the noninteracting system is defined by $(\omega_{po}/2\pi)^2:=(e^2/\hbar a)2\Sigma_k v_{kx}^2\delta(\epsilon_k)$. Using $1/e^2/\hbar\approx 4K\Omega$ and a typical distance in the cubic perovskite structure of $6A$, we find for the ratio A/γ^2 $\approx 1.5\times 10^{-11}$ Ω cm (mol K / m J)^2 at $U=3$. This ratio decreases very slightly as U increases towards large values. This can be seen from Fig. 19, where we plotted $[\partial^2\Sigma/(\partial\omega)^2]$ $(\partial\Sigma/\partial\omega)^2|_{\omega=0}$, which is proportional to A/γ^2.

In infinite dimensions it is possible to make some rigorous statements about the behavior of the Hall coefficient approaching zero temperature. Since vertex corrections can be neglected in the limit of vanishing wave number, the Hall coefficient can be evaluated directly in terms of the exact one-particle Green's function. This statement is not entirely obvious but follows from a restriction of the careful general analysis of Kohno and Yamada[36] to the limit of large lattice coordination.

The diagrams that are neglected in their treatment on the basis of being of higher order in the small damping constant are in fact of higher order in an expansion in $1/d$ relative to the leading terms. At zero temperature, where Fermi liquid applies, one is left with the results of the $U=0$ problem. For an arbitrary band structure one obtains, at $T=0$,

$$R_H=-\frac{a^3}{\hbar e}\frac{\frac{1}{N}\sum_{k,\sigma}\delta(\epsilon_k-\mu_0)\left(v_x^2\frac{\partial v_y}{\partial k_y}-v_y^2\frac{\partial v_y}{\partial k_x}\right)}{\left(\frac{1}{N}\sum_{k,\sigma}\delta(\epsilon_k-\mu_0)v_x^2\right)^2}. \tag{16}$$

It is remarkable that the Hall coefficient at very low temperatures is given by the bare band structure even when the correlations are very strong. This results from the contribution of the quasiparticles to the transport. At high temperatures the resonance disappears and the rigid band picture of Hubbard gives an accurate description of the physics of the model.[23] The Hall number is then holelike for small hole doping. This was observed in the Monte Carlo calculations at high temperatures in the hole-doped Hubbard model.[16] A detailed study of the temperature dependence of the Hall coefficient displaying the change of sign as a function of temperature has been recently carried out by Jarrell and collaborators in Ref. 34.

Equation (16) evaluated in the limit of infinite coordination number yields $R_H=-(2a^3/eD^2)$ $[\mu_0/\rho_0(\mu_0)]$, where $\rho_0(\epsilon)$ is the bare lattice density of states. Using Eq. (2), we obtain, for the Bethe lattice, $R_H=(2\pi a^3/e)[\mu_0/D/\sqrt{1-(\mu_0/D)^2}]$.

However, with respect to experiments, it is more reasonable to evaluate (16) in the spirit of mean-field theory, i.e., for a realistic band structure. As an application, we calculated the Hall coefficient as a function of doping for a three-band model given by $\epsilon_k^{(x)}=-2t(\cos k_y+\cos k_z)$, $\epsilon_k^{(y)}=-2t(\cos k_x+\cos k_z)$, and $\epsilon_k^{(z)}=-2t(\cos k_x+\cos k_y)$. This approach yields a semirealistic description of the $La_{1-x}Sr_xTiO_3$ system. Figure 20 shows the negative inverse Hall coefficient $-1/R_H$ obtained for this case (thick line). For comparison we also included the result for a Bethe lattice with infinite coordination number (thin line). Near half filling the Hall coefficient R_H vanishes in both cases. In the zero-particle limit, however, this quantity remains finite for the more realistic band structure (due to the two-dimensional nature of the model), while it vanishes for the Bethe lattice with infinite coordination number. In the next section our results will be compared with experimental data measured in the $La_{1-x}Sr_xTiO_3$ system.[11]

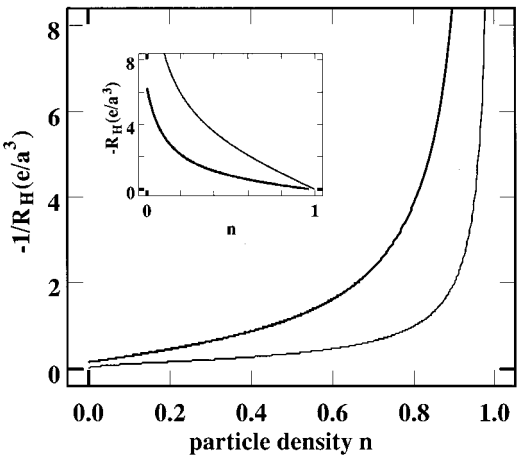

FIG. 20. Doping dependence of the (negative) inverse Hall coefficient $-1/R_H$ at zero temperature. The thick line corresponds to the three-band model mentioned in the text, the thin line to the Bethe lattice with infinite coordination number. The inset contains the Hall coefficient R_H.

IX. CONNECTION WITH EXPERIMENTS: WHEN DOES MEAN-FIELD THEORY WORK?

In this paper we explored in some detail the mean-field theory of the density-driven metal-to-insulator transition. It is important to ascertain the region of validity as well as the applicability to real systems. The doping-induced Mott transition is found in two-different systems: in two-dimensional copper oxide layers as realized in $La_{2-x}Sr_xCuO_x$ and the three-dimensional titanates such as $La_{1-x}Sr_xTiO_3$ and $Y_{1-x}Ca_xTiO_3$.[11,13] When comparing with experiments it is important to bear in mind that these are disordered alloys and the disorder eventually localizes the carriers at low doping levels. The effective strength of the disorder increases with increasing U/D. As a result, it is not possible to approach the density driven Mott transition very closely. In particular this is true for the $Y_{1-x}Ca_xTiO_3$ (Ref. 13) system. Furthermore, the titanates have a perovskite structure with small distortions, implying that the *d* level is threefold degenerate to a good approximation. Therefore the one-band Hubbard model is, strictly speaking, not applicable to these systems.

On the theoretical side, the main limitation of the mean-field theory is the omission of magnetic correlations in the paramagnetic phase. These correlations become very important as the transition is approached, as we know from studies using the large-*N* expansion.[37] The omission of magnetic correlations in the single-particle spectra is the main reason why this approach cannot provide a good description of the cuprate superconductors. This can be seen by comparing the specific heat vs doping curves of the large-*d* Hubbard model[15] with the experimental results of Loram *et al.*[38] Mean-field theory predicts $\gamma \sim \delta^{-1}$, while experiments in the cuprates clearly indicate the opposite trend.

The mean-field approach, however, is quite useful for understanding the physical properties of three-dimensional transition-metal oxides. The physical reason for the success of the mean-field theory for these systems is related to their orbital degeneracy. Orbital degeneracy reduces the relative importance of the magnetic correlations in the paramagnetic phase. In an orbitally degenerate system, there is a competition between ferromagnetic and antiferromagnetic exchange interactions among different spin and orbital configurations. This results in an effective magnetic frustration. The energy difference between different orbital-spin orderings is quite small and results in a very small magnetic transition temperature at half filling. This is confirmed by the magnitude of the magnetic ordering temperature, which is of the order of 1300 K in the quasi-two-dimensional cuprates, but only about 150 K in the cubic titanates. The one-band model in the limit of infinite dimensions can capture the weakening of the effective magnetic couplings (and the very low ordering temperatures) when defined on very frustrated lattices.

In the light of the previously mentioned caveats, we limit ourselves to a qualitative comparison of our theoretical results with the measurements of Tokura and co-workers.[11,13,39] We find good agreement with respect to various physical quantities.

Mass enhancement. It was established in Ref. 15 that the quasiparticle residue scales to zero as the Mott transition is approached with decreasing hole doping, causing a divergence of the specific-heat mass, in quantitative agreement with the experiments performed on $La_{1-x}Sr_xTiO_3$.[11] The compound $La_{1-x}Ca_xYO_3$ has a larger value of U/D, which allows us to test the dependence of the effective mass $m^\star = f(U/D)\delta^{-1}$ on the ratio U/D. From Fig. 10 we expect the linear term in the specific heat to increase as U/D is increased. The same qualitative behavior is found in the experiments: For $x=0.5$, we have $\gamma = 5.2(\mathrm{mJ}/K^4\mathrm{mol}^2)$ for $La_{1-x}Sr_xTiO_3$ and $\gamma = 8.2(\mathrm{mJ}/K^4\mathrm{mol})^2$ for $Y_{1-x}Ca_xTiO_3$).[13] We stress again that the opposite behavior (the specific-heat coefficient *vanishes* near zero doping) is seen in the copper oxide systems such as $La_{2-x}Sr_xCuO_4$, so the mean-field approach to the Hubbard model (or perhaps the Hubbard model itself[40]) is not applicable in this case.

Transfer of spectral weight. As one dopes the Mott insulator the spectral weight of the upper Hubbard band is reduced, while at the same time new states are created within the gap. The details of the photoemission spectra in $La_{1-x}Sr_xTiO_3$ cannot be described by the Hubbard model without taking into account the effects of inhomogeneities on the surface.[41] Nevertheless, optical experiments can probe the transfer of spectral weight to low energies.[39] Measurements in $R_{1-x}Ca_xTiO_3$, with $R=$ La, Nd, Sm, or Y, have established experimentally that the weight of the Drude peak in the optical conductivity is proportional to the doping δ. The proportionality constant increases as U/D decreases, in agreement with the results in Figs. 10 and 8 and the relation between the Drude weight and the quasiparticle residue. A more careful study of the optical conductivity is necessary, however, for a quantitative comparison with these experiments. In particular the proportionality constant does not diverge at U_c in our treatment.

Wilson ratio. Another physically relevant quantity is the behavior of the Wilson ratio as a function of doping and of D/U. For U close to U_c this question was examined in Ref. 15 in the context of the one-band Hubbard model where it was shown that the Wilson ratio goes to zero very close to half filling, but it is close to one for dopings larger than 0.05. In an orbitally degenerate situation, there are important orbital contributions to the susceptibility even in the noninteracting limit. For the case of the cubic perovskites

$R_{1-x}Ca_xTiO_3$, taking the magnetic moment operator to $2S+L$ and restricting our attention to the threefold degenerate d band, one obtains in the limit of small number of particles

$$\frac{\chi}{\gamma}\Big/\frac{3\mu_B^2}{\pi^2 k_B^2}=1+\frac{\frac{2}{3}\sum_k \frac{f(\epsilon_{1k})-f(\epsilon_{2k})}{\epsilon_{1k}-\epsilon_{2k}}}{\sum_k f'(\epsilon_{1k})}, \tag{17}$$

which is therefore larger than one. $\epsilon_{1k},\epsilon_{2k}$ are two of the bands considered in the discussion of the Hall coefficient. Experimentally the Wilson ratio is close to 2 for all dopings in $La_{1-x}Sr_xTiO_3$. For $Y_{1-x}Ca_xTiO_3$ the Wilson ratio is 2 for large doping and increases slightly as the doping is reduced [for $x=0.5$ we obtain $R\approx 3.2(3\mu_B^2/\pi^2 k_B^2)$]. This trend is the same as the trend we find in our generalized Wilson ratio $R_g:=(\chi_{\rm loc}/\gamma)/(\chi_0/\gamma_0)$. The generalized Wilson ratio depends weakly on doping and its value increases slightly with U ($R_g\approx 2.6$ for $U=3$ and $R_g\approx 2.75$ for $U=10$).

Low-temperature resistivity. In our treatment the low-temperature resistivity obeys $\rho=AT^2$, where A is proportional to γ^2. Earlier work[25] estimated $A/\gamma^2\approx 1.5\times 10^{-11}$ Ω cm(mol K/mJ)^2 at $U=U_c$, which was in good agreement with experimental data for $La_{1-x}Sr_xTiO_3$ [10^{-11} Ω cm(mole K/mJ)^2]. Here we showed that A/γ^2 *decreases* with increasing U. This prediction cannot be tested in $Y_{1-x}Ca_xTiO_3$, because its resistivity has a T^3 dependence at the only composition where it has been measured ($x=0.42$), which is very close to the disorder-induced metal-insulator transition.

Hall coefficient. For hole doping the Hall coefficient at $T=0$ is electronlike and essentially unrenormalized from the band-structure value. The results for the three-band model treated in Sec. VIII should be compared with experimental data for the $La_{1-x}Sr_xTiO_3$ system. From experiments it is known that $n=(1-x)$. Assuming a lattice constant of $6A$, the mean-field approach yields the data plotted in Fig. 21 (full line). The closed circles indicate the experimental data. At large dopings ($x>0.3$), there is a reasonable qualitative agreement. Also, the order of magnitude is the same in both cases. Note, however, that the Hall coefficient is proportional to a^3, so that $|R_H|$ depends strongly on the choice for a. Deviations from the measured data are large at small doping, where the theoretically determined inverse Hall coefficient diverges. Such a divergence cannot be seen in the experiments. However, there is still a superlinear enhancement of $|1/R_H|$ in this region. The Hall coefficient found in $Y_{1-x}Ca_xTiO_3$ is of the same order of magnitude as in $La_{1-x}Sr_xTiO_3$ (e.g., for $x=0.5$ we have $-1/R_H\approx 0.76\times 10^{-22}$ cm$^{-3}/e$ in $La_{1-x}Sr_xTiO_3$ and $-1/R_H\approx 1.0\times 10^{-22}$ cm$^{-3}/e$ in $Y_{1-x}Ca_xTiO_3$). Deviations may be explained by differences in the lattice constants and by the presence of disorder.

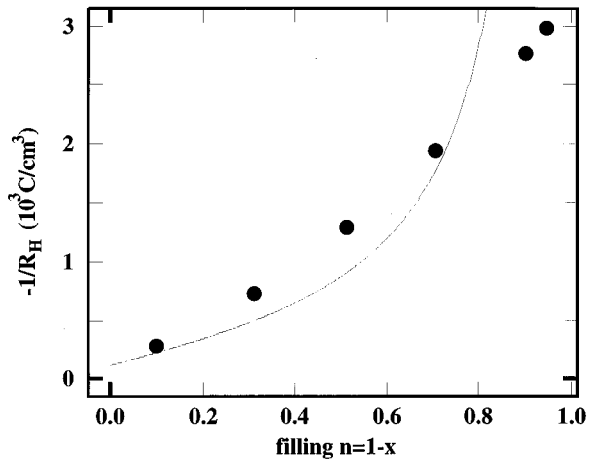

FIG. 21. Inverse Hall coefficient $-1/R_H$: data from mean-field theory (full line) in comparison with experimental data of $La_{1-x}Sr_xTiO_3$ (closed circles).

In this paper we have discussed various aspects of the density-driven Mott transition. When comparing the behavior of various physical quantities as a function of U/D we find satisfactory agreement between the mean-field theory and experimental data.

The next step towards a realistic description of transition-metal oxides would be to introduce a more realistic density of states as well as crystal structures and the orbital degeneracies characteristic for these systems. From a physical point of view, frustration should emerge as a result of the orbital degeneracy[31] rather than having to be put in by hand, as a geometric property of the lattice, as is done in the context of the one-band description. We expect, however, that the main qualitative conclusions of the mean-field theory in the paramagnetic phase will not be changed by the orbital degeneracy. Work along these lines is already under way. In this respect the recent success of the mean-field theory in predicting the results of optical experiments on V_2O_3 is very encouraging.[10]

ACKNOWLEDGMENT

This work has been supported by the National Science Foundation Grant No. DMR 95-29138.

[1] N. F. Mott, Proc. R. Soc. London Ser. A **62**, 416 (1949).
[2] W. Metzner and D. Vollhardt, Phys. Rev. Lett. **62**, 324 (1989).
[3] A. Georges and G. Kotliar, Phys. Rev. B **45**, 6479 (1992).
[4] A. Georges, G. Kotliar, and Q. Si, Int. J. Mod. Phys. B **6**, 705 (1992).
[5] M. Jarrell, Phys. Rev. Lett. **69**, 168 (1992)
[6] S. Ogawa, J. Appl. Phys. **50**, 2308 (1979).
[7] I. H. Inoue *et al.*, Phys. Rev. Lett. **74**, 2539 (1995).
[8] D. B. McWhan, A. Menth, J. P. Remeika, W. F. Brinkman, and T. M. Rice, Phys. Rev. B **7**, 1920 (1973).
[9] H. Kuwamoto, J. M. Honig, and J. Appel, Phys. Rev. B **22**, 2626 (1980).
[10] G. A. Thomas *et al.*, Phys. Rev. Lett. **73**, 1529 (1994); M. Rozenberg *et al.*, *ibid.* **75**, 105 (1995).
[11] Y. Tokura, Y. Taguchi, Y. Okada, Y. Fujishima, T. Arima, K. Kumagai, and Y. Iye, Phys. Rev. Lett. **70**, 2126 (1993).

[12] A. Fujimori, Phys. Rev. Lett. **69**, 1796 (1992).
[13] Y. Okimoto, T. Katsufuji, and Y. Tokura, Phys. Rev. B **51**, 9581 (1995).
[14] G. Kotliar and M. Rozenberg, in *the Hubbard Model*, edited by D. Baeriswyl, D. K. Campbell, J.M.P. Carmelo, F. Guinea, and E. Louis (Plenum, New York, 1995), p. 155.
[15] M. J. Rozenberg, G. Kotliar, and X. Y. Zhang, Phys. Rev. B **49**, 10 181 (1994).
[16] M. Jarrell and T. Pruschke, Phys. Rev. B **49**, 1458 (1993); T. Pruschke, D. L. Cox, and M. Jarrell, Europhys. Lett. **21**, 593 (1993); Phys. Rev. B **47**, 3553 (1993).
[17] D. Fisher, G. Kotliar, and G. Moeller, Phys. Rev. B **52**, 17 112 (1995).
[18] M. Caffarel and W. Krauth, Phys. Rev. Lett. **72**, 1545 (1994); Q. Si, M. Rozenberg, G. Kotliar, and A. Ruckenstein, *ibid.* **72**, 2761 (1994).
[19] M. Rozenberg, X. Y. Zhang, and G. Kotliar, Phys. Rev. Lett. **69**, 1236 (1992).
[20] A. Georges and W. Krauth, Phys. Rev. B **48**, 7167 (1993).
[21] A. Georges and W. Krauth, Phys. Rev. Lett. **69**, 1240 (1992).
[22] M. J. Rozenberg, G. Moeller, and G. Kotliar, Mod. Phys. Lett. B **8**, 535 (1996).
[23] For recent reviews see A. Georges, G. Kotliar, W. Krauth, and M. Rozenberg, Rev. Mod. Phys. **68**, 13 (1996). Th. Pryskhe M. Janell and J. Freericks, Adv. Phys. **44**, 187 (1995). G. Kotliar, in *Metal-Insulator Trasition Revisited*, edited by P. P. Edwards and C. N. R. Rao (Taylor and Francis, London, 1995), p. 317.
[24] X. Y. Zhang, M. J. Rozenberg, and G. Kotliar, Phys. Rev. Lett. **70**, 1666 (1993).
[25] G. Moeller, Q. Si, G. Kotliar, M. Rozenberg, and D. Fisher, Phys. Rev. Lett. **74**, 2082 (1995).
[26] H. Kajueter and G. Kotliar, Phys. Rev. Lett. (to be published).
[27] D. M. Edwards and J. A. Hertz, Physica B **163**, 527 (1990); S. Wermbter and G. Czycholl, J. Phys. Condens. Matter **7**, 7335 (1995).
[28] Roy G. Gordon, J. Math. Phys. **9**, 655 (1968).
[29] W. Nolting and W. Borgiel, Phys. Rev. B **39**, 6962 (1989).
[30] A. Martin-Rodero, F. Flores, M. Baldo, and R. Pucci, Solid State Commun. **44**, 911 (1982); A. Martin-Rodero, E. Louis, F. Flores, and C. Tejedor, Phys. Rev. B **33**, 1814 (1986).
[31] C. Castellani, G. Kotliar, R. Raimondi, M. Grilli, Z. Wang, and M. Rozenberg, Phys. Rev. Lett. **69**, 2009 (1992).
[32] H. Jichu, T. Matsuura, and Y. Kuroda, J. Phys. Soc. Jpn. **58**, 4280 (1989); **59**, 2820 (1990).
[33] E. Dagotto, Rev. Mod. Phys. **66**, 763 (1994).
[34] M. Jarrell and T. Pruschke, Z. Phys. B **90**, 187 (1993).
[35] Q. Qin, and G. Czycholl, Physica B **199-200**, 219 (1994).
[36] H. Kohno and K. Yamada, Prog. Theor. Phys. **80**, 623 (1998).
[37] M. Grilli and G. Kotliar, Phys. Rev. Lett. **64**, 1170 (1990).
[38] J. W. Loram *et al.*, Physica C **235**, 134 (1994); **162**, 498 (1989); Phys. Rev. Lett. **71**, 1740 (1993).
[39] T. Katsufuji, Y. Okimoto, and Y. Tokura, Phys. Rev. Lett. **75**, 3497 (1995).
[40] M. Imada, J. Phys. Soc. Jpn **62**, 1105 (1993); N. Furukawa and M. Imada, *ibid.* **60**, 3604 (1991).
[41] D. D. Sarma, S. Barman, H. Kajueter, and G. Kotliar (unpublished).